CrossMark

# The Lobster Eye Imager for Astronomy Onboard the SATech-01 Satellite

Z. X. Ling[1,2], X. J. Sun[3], C. Zhang[1,2], S. L. Sun[3], G. Jin[4], S. N. Zhang[1,2,5], X. F. Zhang[6], J. B. Chang[3], F. S. Chen[3], Y. F. Chen[3],
Z. W. Cheng[3], W. Fu[3], Y. X. Han[3], H. Li[3], J. F. Li[3], Y. Li[3], Z. D. Li[3], P. R. Liu[3], Y. H. Lv[3], X. H. Ma[3], Y. J. Tang[3], C. B. Wang[3],
R. J. Xie[3], Y. L. Xue[3], A. L. Yan[3], Q. Zhang[3], C. Y. Bao[1], H. B. Cai[1], H. Q. Cheng[1], C. Z. Cui[1], Y. F. Dai[1], D. W. Fan[1], H. B. Hu[1],
J. W. Hu[1], M. H. Huang[1], Z. Q. Jia[1], C. C. Jin[1], D. Y. Li[1], J. Q. Li[1], H. Y. Liu[1], M. J. Liu[1], Y. Liu[1], H. W. Pan[1], Y. L. Qiu[1],
M. Sugizaki[1], H. Sun[1], W. X. Wang[1], Y. L. Wang[1], Q. Y. Wu[1], X. P. Xu[1], Y. F. Xu[1], H. N. Yang[1], X. Yang[1], B. Zhang[1],
M. Zhang[1], W. D. Zhang[1], Z. Zhang[1], D. H. Zhao[1], X. Q. Cong[4], B. W. Jiang[4], L. H. Li[4], X. B. Qiu[4], J. N. Sun[4], D. T. Su[4],
J. Wang[4], C. Wu[4], Z. Xu[4], X. M. Yang[4], S. K. Zhang[4], Z. Zhang[4], N. Zhang[7], Y. F. Zhu[7], H. Y. Ban[6], X. Z. Bi[6], Z. M. Cai[6],
W. Chen[6], X. Chen[6], Y. H. Chen[6], Y. Cui[6], X. L. Duan[6], Z. G Feng[6], Y. Gao[6], J. W. He[6], T. He[6], J. J. Huang[6], F. Li[6], J. S. Li[6],
T. J. Li[6], T. T. Li[6], H. Q. Liu[6], L. Liu[6], R. Liu[6], S. Liu[6], N. Meng[6], Q. Shi[6], A. T. Sun[6], Y. M. Wang[6], Y. B. Wang[6], H. C. Wu[6],
D. X Xu[6], Y. Q Yang[6], Y. Yang[6], X. S. Yu[6], K. X. Zhang[6], Y. L. Zhang[6], Y. H. Zhang[6], Y. T. Zhang[6], H. Zhou[6], X. C. Zhu[6],
J. S. Cheng[8], L. Qin[8], L. Wang[8], Q. L. Wang[8], M. Bai[9], R. L. Gao[9], Z. Ji[9], Y. R. Liu[9], F. L. Ma[9], Y. J. Shi[9], J. Su[9], Y. Y. Tan[9],
J. Z. Tong[9], H. T. Xu[9], C. B. Xue[9], G. F. Xue[9], and W. Yuan[1,2]
[1] National Astronomical Observatories, Chinese Academy of Sciences, Beijing 100101, China; chzhang@nao.cas.cn
[2] School of Astronomy and Space Science, University of Chinese Academy of Sciences, Beijing 100049, China
[3] Shanghai Institute of Technical Physics, Chinese Academy of Sciences, Shanghai 200083, China; sunxiaojin@mail.sitp.ac.cn
[4] North Night Vision Technology Co., LTD, Nanjing 211106, China
[5] Institute of High Energy Physics, Chinese Academy of Sciences, Beijing 100049, China
[6] Science and Technology on Low-Light-Level Night Vision Laboratory, Xi'an 710065, China
[7] Innovation Academy for Microsatellites, Chinese Academy of Sciences, Shanghai 201204, China
[8] Institute of Electrical Engineering, Chinese Academy of Science, Beijing 100190, China
[9] National Space Science Center, Chinese Academy of Science, Beijing 100190, China

## Abstract

The Lobster Eye Imager for Astronomy (LEIA), a pathfinder of the Wide-field X-ray Telescope of the Einstein Probe mission, was successfully launched onboard the SATech-01 satellite of the Chinese Academy of Sciences on 2022 July 27. In this paper, we introduce the design and on-ground test results of the LEIA instrument. Using state-of-the-art Micro-Pore Optics (MPO), a wide field of view of 346 square degrees ($18°\!.6 \times 18°\!.6$) of the X-ray imager is realized. An optical assembly composed of 36 MPO chips is used to focus incident X-ray photons, and four large-format complementary metal-oxide semiconductor (CMOS) sensors, each of size 6 cm × 6 cm, are used as the focal plane detectors. The instrument has an angular resolution of $4'$–$8'$ (in terms of FWHM) for the central focal spot of the point-spread function, and an effective area of 2–3 $cm^2$ at 1 keV in essentially all the directions within the field of view. The detection passband is 0.5–4 keV in soft X-rays and the sensitivity is $2$–$3 \times 10^{-11}\, erg\, s^{-1}\, cm^{-2}$ (about 1 milliCrab) with a 1000 s observation. The total weight of LEIA is 56 kg and the power is 85 W. The satellite, with a design lifetime of 2 yr, operates in a Sun-synchronous orbit of 500 km with an orbital period of 95 minutes. LEIA is paving the way for future missions by verifying in flight the technologies of both novel focusing imaging optics and CMOS sensors for X-ray observation, and by optimizing the working setups of the instrumental parameters. In addition, LEIA is able to carry out scientific observations to find new transients and to monitor known sources in the soft X-ray band, albeit with limited useful observing time available.

*Key words:* instrumentation: detectors – space vehicles: instruments – telescopes – X-rays: general

## 1. Introduction

X-ray wide-field monitoring observations in time-domain have been playing an important role in discovering and understanding the X-ray Universe. The Wolter-I telescopes, which are commonly used in X-ray astronomy, are inconvenient for use as monitoring-type instruments, however, due to their small field of view (FoV) of typically 1° or less. An

interesting lobster-eye design was proposed by Angel (1979), which can in principle realize both a large FoV and relatively high sensitivity, by making use of Micro-Pore Optics (MPO). In theory, the imaging properties of such an optic remain invariant in essentially all the directions across the entire FoV except close to the edges. This means that, theoretically, there is almost no vignetting effect over most of the FoV. In the past

decades, extensive efforts have been made in the study of lobster-eye optics and the development of the MPO techniques (Wilkins et al. 1989; Chapman et al. 1991; Kaaret et al. 1992; Fraser et al. 1992, 1993; Peele et al. 1996; Brunton et al. 1999; Collier et al. 2015; Willingale et al. 2016; Hudec et al. 2017). Despite these efforts, no in-flight observations made by X-ray focusing lobster-eye telescopes with a truly large FoV (i.e., the order of 100 square degrees or larger) have been achieved until recently.

The Einstein Probe (EP) (Yuan et al. 2016, 2018, 2022) of the Chinese Academy of Sciences (CAS) is a space mission for time-domain astronomy equipped with a wide-field X-ray monitor built from lobster-eye MPO. The EP mission is an international collaboration project led by the CAS with participation from the European Space Agency (ESA), the Max-Planck Institute for Extraterrestrial Physics (MPE) and the French Space Agency (CNES). The mission was formally adopted in 2017 December and is aimed for launch at the end of 2023. EP has two payloads, the Wide-field X-ray Telescope (WXT) making use of lobster-eye MPO (Z. X. Ling et al. 2023, in preparation) and the Follow-up X-ray Telescope (FXT) of the Wolter-I type (Chen et al. 2020). EP-WXT is composed of 12 identical modules and has an overall FoV as large as 3600 sq.deg. Besides lobster-eye MPO, another novel technique employed for WXT is a large array of complementary metal-oxide semiconductor (CMOS) sensors used as focal plane detectors (Yuan et al. 2022).

A pathfinder for the EP-WXT and telescopes of this kind was proposed in 2019 by the EP team. The aims are to verify the in-orbit performance of both the MPO and CMOS components used for the EP-WXT, and to optimize the operational instrumental parameters in space. The pathfinder was successfully launched on 2022 July 27, piggybacked as one of the scientific payloads onboard the SATech-01 satellite. The instrument was subsequently named Lobster Eye Imager for Astronomy (LEIA). LEIA will soon complete the performance verification (PV) and in-orbit calibration phase and is starting to carry out scientific observations as a wide-field X-ray monitor. This paper introduces the LEIA instrument. The design of LEIA is presented in Section 2. The simulated performance and the ground test result are summarized in Section 3. The LEIA experiment is described in Section 4. The result of LEIA and current status are shown in Section 5, followed by a summary in Section 6.

## 2. Instrumental Design

LEIA is a test model of one of the 12 WXT modules onboard the EP satellite. Here we summarize the basic design of LEIA. For an account of the technical details of the WXT instrument, see Z. X. Ling et al. (2023, in preparation). To achieve both a large FoV and focused imaging, LEIA relies on a lobster-eye MPO to focus incident X-ray photons. An array of mosaics of
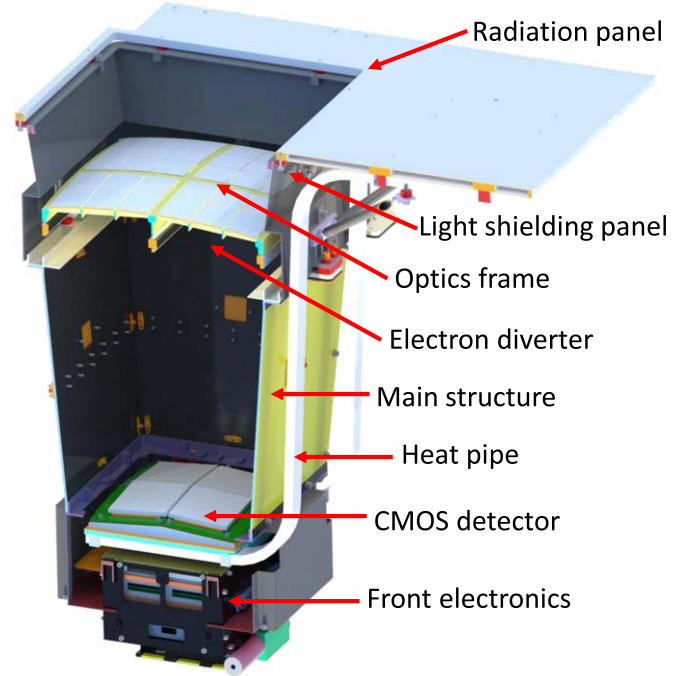


**Figure 1.** Schematic view of LEIA.

$6 \times 6 = 36$ plates, each of $4.25\,\mathrm{cm} \times 4.25\,\mathrm{cm}$ in size and 2.5 mm thickness, forms the focusing optical system. The designed focal length of the MPO optics is 375 mm, with a deviation of about $\pm 1.5\%$. The optical system is divided into four quadrants, each composed of $3 \times 3$ MPO plates. On the focal sphere corresponding to each of the optical quadrants, a large-format CMOS sensor of $6\,\mathrm{cm} \times 6\,\mathrm{cm}$ in size is used as a detector to collect X-ray photons. Although the CMOS detectors are planar, they are tilted with respect to each other on the focal plane to best fit the curved focal surface. Figure 1 illustrates the shape of the focal plane. The total FoV of the imager is $18°\!.6 \times 18°\!.6$. A schematic view of the imaging system can be found in Figure 1 (left panel) in Zhang et al. (2022).

To our knowledge, there had been no CMOS sensors operating as X-ray astronomical detectors in orbit prior to LEIA. The CMOS sensors are back-illuminated, with a read-out frame rate of 20 Hz. The pixel size is $15\,\mu\mathrm{m} \times 15\,\mu\mathrm{m}$, much smaller than the angular resolution of the mirror assembly. The X-ray performance of the CMOS sensors, very similar to those used for LEIA (the only difference is that the ones used for LEIA are coated with a layer of aluminum), can be found in Wu et al. (2022). The built-in thermal control of the module is applied to keep the temperature of the optical assembly at $6°C$. The CMOS detectors are designed to operate at a temperature of $-30°C$, which is optimized to achieve good detector performance while minimizing the demand for power resources. To prevent optical and ultraviolet light from

**Table 1**
Instrument Specifications of LEIA

| Optic | 36 MPO plates |
|---|---|
| Detector | Four 6 cm × 6 cm CMOS sensors |
| Field of View | 346 square degrees |
| Focal length | 375 mm |
| Angular resolution | 4′–8′ (FWHM, measured) |
| Energy band | 0.5–4 keV |
| Energy resolution | 125 ± 2 eV at 1.25 keV |
| Time resolution | 50 ms |
| Source positioning accuracy[a] | <1′ |
| Weight | 53 kg (total) |
| Power | 85 W |

**Note.**
[a] In the detector coordinates.

reaching the detectors in orbit, a 200 nm-thick aluminum layer is coated on the surface of the CMOS sensors. Moreover, an 80 nm-thick aluminum layer is also coated directly on the MPO plates. The specifications of LEIA are listed in Table 1.

The design of the imager is drawn in Figure 1.

At the top is a radiating panel that is connected to the detector unit with a heat pipe to cool the detectors down to the required working temperature ($-30°$). An optical baffle is mounted above the optical assembly, connecting the radiation panel. An electron diverter is mounted beneath the optical assembly to deflect low-energy electrons in orbit. The deflecting efficiency is greater than 97% for electrons of energy less than 1 MeV (Wang et al. 2020). The main mechanical structure connects the optical assembly and the focal plane unit. The detector and its front-end electronics box are located at the bottom of the instrument. The vibration frequency of the whole structure is 280 Hz, far beyond the first-order frequency of the satellite platform. This main component of the imager weighs 26 kg with a power of 25 W. The overall size is 695 mm × 540 mm × 698 mm. An exterior view of the lobster-eye imager is shown in Figure 2.

In addition to the upper main structure, an independent and auxiliary electronics control box (ECB) is attached to the module inside the satellite platform for the control of the instrument and its temperature. A transient triggering board is integrated into the ECB to realize the algorithm to find new transients in real time. The alert message of triggers will be transmitted to the ground by the Beidou navigation system in real time. The ECB will package all the scientific and housekeeping data and send them to the satellite storage disk. The estimated data rate for LEIA is about 5 GB per day. The weight of the ECB is 27 kg and the



**Figure 2.** Picture of the LEIA instrument after engineering integration.

power is 60 W, making a total weight of 53 kg and a total power of 85 W for the whole payload.

LEIA was developed jointly by the National Astronomical Observatories (NAOC) and the Shanghai Institute of Technical Physics (SITP), CAS. The mirror assembly was developed at the X-ray Imaging Lab of NAOC, and the complete WXT module was engineered by integrating the mirror assembly, the detector unit and thermal control at SITP. The MPO plates were manufactured by North Night Vision Technology Company (NVVT) in collaboration with and jointly sponsored by the CAS and the National Natural Science Foundation of China.

## 3. Performance and On-ground Calibration

### 3.1. Simulated Performance

The performance of the EP WXT module has been studied extensively by both simulations and on-ground tests and calibration. A Geant4 model was built to simulate its performance and the background in orbit (Zhao et al. 2017). The simulated image of the point-spread function (PSF) and the effective area of the optical system at 1 keV are displayed in
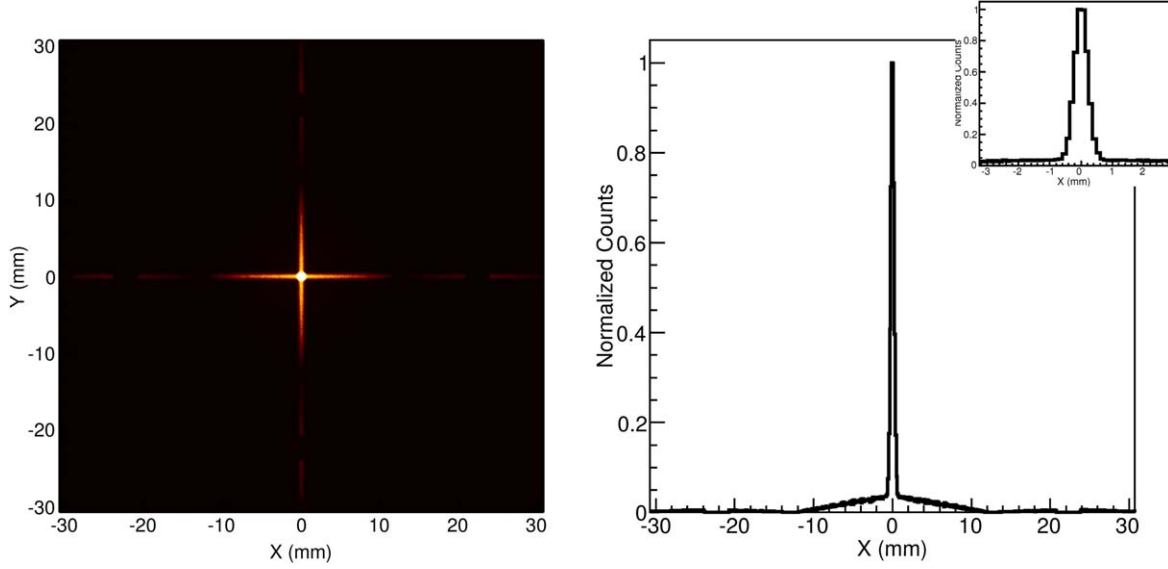
**Figure 3.** The simulated PSF at 1 keV for the LEIA instrument. The focal length is 375 mm for the MPO optical assembly.
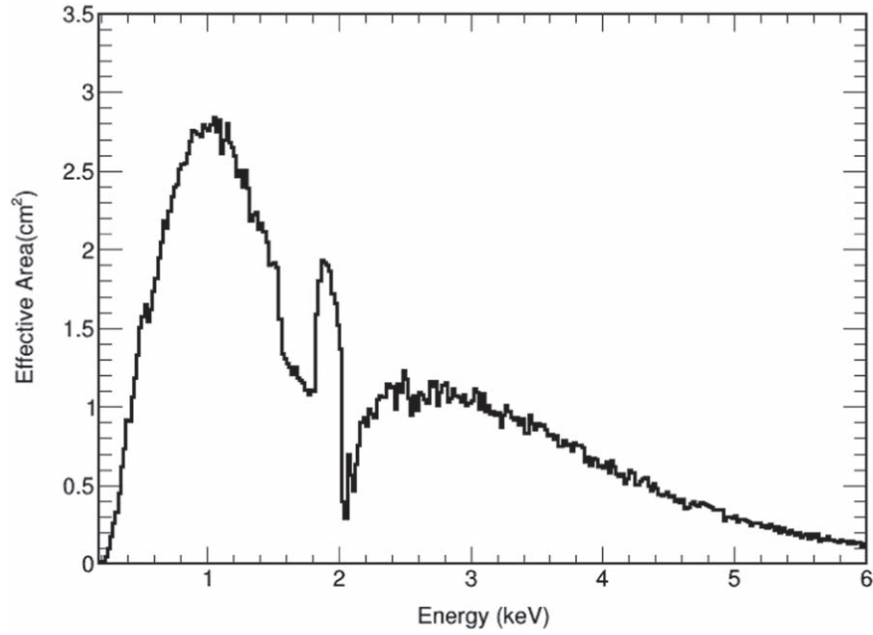


**Figure 4.** The total effective area of the LEIA instrument with a central spot of radius of 6′. This area includes the mirror assembly and the quantum efficiency of the detector. The dip near 1.5 keV is due to the absorption of the aluminum coating. The increase near 1.8 keV is due to the absorption edge of silicon. The dip near 2 keV is due to the M absorption edge of iridium. A thin layer of iridium is coated on the channel surface of the MPO chips to boost the reflection efficiency of soft X-ray.

Figures 3 and 4, respectively. As a distinctive feature of the lobster-eye MPO optics, the PSF assumes a cruciform shape with a bright central focal spot (Angel 1979). The size of the central focal spot is commonly used to represent the PSF and hence the angular resolution of the lobster-eye optics. The angular resolution of the mirror assembly is expected to be around 5′ in terms of full width at half maximum (FWHM) in

most directions within the FoV. The sigma of a Gaussian fitting of the core region is about 1′–2′, as depicted in the right bottom panel of Figure 5. This PSF value leads to a source localization accuracy of 1′ for a source with about 200 counts (statistical errors in the detector coordinates). Using a photometric aperture of a circle of 6′ radius (corresponding to 3σ of the core region of PSF) around the central spot, the simulated
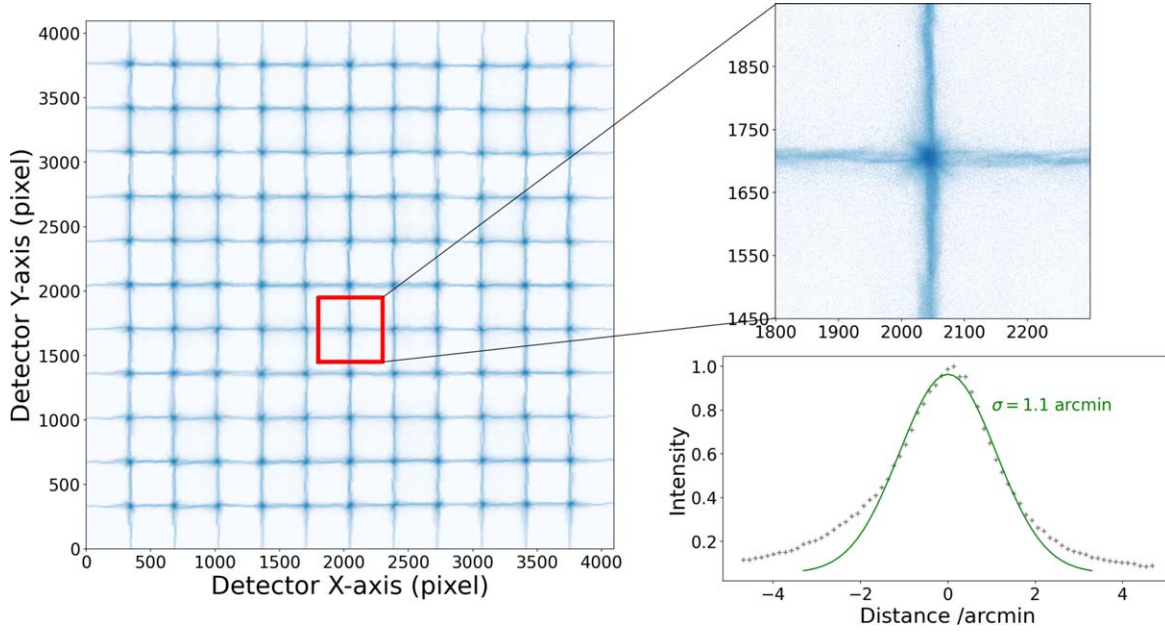
**Figure 5.** Mosaicked image of an 11 × 11 array of the images of the PSF of the first quarter of the optical assembly at NAOC. The right top panel shows the zoom-in image of a typical PSF. The right bottom panel depicts the 1D profile of the PSF. Here, we use a Gaussian function to fit the central part of the profile. The fitted Gaussian standard deviation is only $1'.1$.

effective area is about 3.5 cm$^2$ at 1 keV (for the optics only, without taking into account the focal plane detector). This is consistent with the on-ground calibration result (H. Q. Cheng et al. 2023, in preparation). Figure 4 plots the effective area of LEIA in the energy band 0.3–6 keV.

The in-orbit background, including the cosmic diffuse X-ray emission and detector background, has also been simulated by considering the charged particle environment. It should be noted that in these simulations, the orbit of the EP satellite was adopted, which is different from that of LEIA. The diffuse cosmic X-ray photons contribute 0.14 count s$^{-1}$ cm$^{-2}$ to the background, whereas the particle-induced background is 0.17 count s$^{-1}$ cm$^{-2}$, resulting in a total background rate of ~0.31 count s$^{-1}$ cm$^{-2}$. Based on these background results, the expected sensitivity of LEIA is estimated to be about 2–3 × 10$^{-11}$ erg s$^{-1}$ cm$^{-2}$, or ~1 milliCrab for a typical observation duration of 1000 s.[10] The details and results of the background simulation can be found in Zhao et al. (2018).

The oversampling of the PSF with the small pixel size, the high frame rate of the CMOS detectors, and the small effective area make the instrument almost free from pile-up effects even for X-ray sources as bright as Sco X-1.

### 3.2. Instrument Tests and Calibrations

The instrument tests and calibrations were carried out in two stages. First, the lobster-eye mirror assembly and the CMOS

---
[10] http://ep.bao.ac.cn

sensors were tested and calibrated separately. When the complete telescope module was engineered, end to end tests and calibrations were performed in order to achieve a thorough understanding of the instrument performance. The detailed setup, procedure and results of these calibration experiments are topics of separate papers and will be presented elsewhere. In this paper, we briefly introduce the tests and calibrations carried out for LEIA and only summarize the main results.

The mirror assembly was calibrated at the PANTER facility of MPE (Freyberg et al. 2005) in 2021 April by a joint team from MPE and University of Leicester under the collaboration framework with ESA. Afterwards, its optical performance was tested twice at NAOC, one before and another after a qualification vibration test in 2021 September. In these two tests, the mirror assembly was illuminated by an X-ray beam from a point-like X-ray source about 15 m away. A Ti target X-ray tube was used to produce a soft continuum X-ray spectrum with a high voltage setting of 6 KV. The source was scanned in an 11 × 11 array of different directions within the FoV of each of the four quadrants by changing the aspects of the mirror assembly. Figure 5 features a mosaicked 11 × 11 array of images of the PSF over one quadrant of the FOV of the mirror assembly. The right top panel of Figure 5 shows a typical PSF of the optics. The right bottom panel displays the projection of the PSF. A Gaussian function is used to fit the central part of the projection to represent the angular resolution. (The king function could fit the curve better, especially in the shoulder of the curve.) The measured PSF values are in the
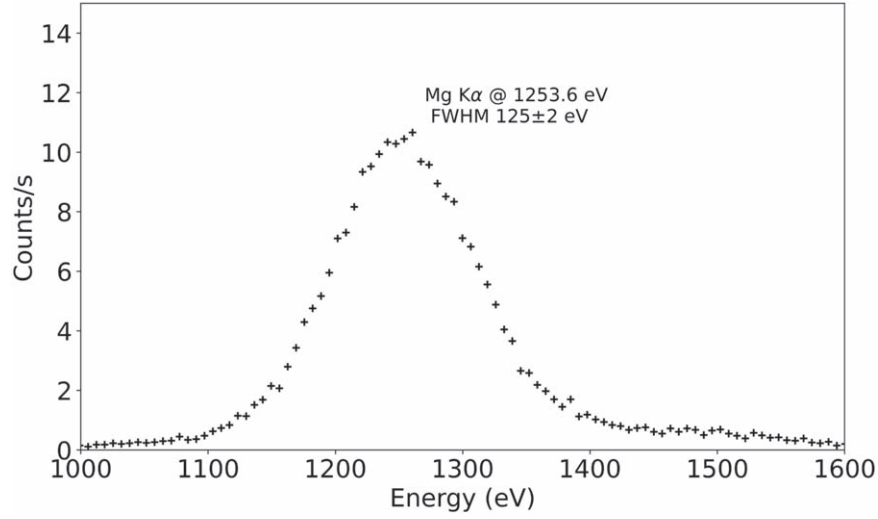
**Figure 6.** Spectrum of the Mg Ka line at 1.25 keV measured in the calibration undertaken at IHEP/CAS. The energy resolution is $125 \pm 2$ eV.

range of 4′–8′ in FWHM and about 85% are less than 5′. The measured PSF values are generally consistent with the Geant4 simulation results.

Unfortunately, for three of the overall 36 MPO plates, their foci were found to be misaligned from the focal point of the module, due to the incorrect plate parameters used in the mounting. However, the effect of these misalignments is limited and affects the imaging quality of two localized areas in two quadrants, which amounts to only 10% of the total FoV for the module. This misalignment could be corrected by a series of full scan observations across the whole FoV.

In 2021 December, an end-to-end test and calibration campaign for the complete module was carried out at the 100 m test facility (Wang et al. 2022) at Institute of High Energy Physics (IHEP), CAS. The campaign included calibration of the imaging quality and PSF, imaging offset, effective area and energy resolution. X-ray photons from emission lines of several targets, including Mg, Cu, Si and Ti, were applied. X-ray events were extracted from the CMOS sensors, which showed various patterns of pixels hit by photons (see Wu et al. 2022 for the definition of the event pixel patterns for CMOS sensors). Single, double, triple and quartic events were recorded as true X-ray events. Other grades were excluded during data extraction. The energy resolution (FWHM) was $125 \pm 2$ eV at 1.25 keV and $175 \pm 2$ eV at 4.5 keV. As an example, the detector spectrum of the Mg Ka line (1.25 keV) is shown in Figure 6. The transmission of optical light through the aluminum filters, considering the layers on the CMOS and MPO, was measured to be less than $10^{-6}$.

The effective area of the complete module was also calibrated in a $11 \times 11$ grid of directions. The measured effective areas are in the range of 2–3 cm$^2$ at 1.25 keV across the entire FoV, except at the edges of the FoV. Theoretically,

ideal lobster-eye optics predict the same PSF shape and effective area in all the directions (except at the edge). The mild non-uniformity, i.e., a decrease of the effective area or a change of the PSF in some of the directions, across the FoV, as measured for this instrument, can easily be understood and can be reproduced by simulations. The non-uniformity of the PSF arises from these factors: the imperfectness during the manufacturing and the mounting of the optics, and the mismatch between the flat detector plane and the spherical focal plane. The obscuration of the mounting frame between the individual MPO plates for the incident X-ray photons would produce a smaller effective area in some directions than the nominal $\sim 3$ cm$^2$ of the MPO plates, causing the non-uniformity of effective area except for the edge region.

To summarize, results of the on-ground calibrations are generally consistent with those of the simulations. The distributions of the PSF and effective areas are basically uniform (showing no substantial variations) across the whole FoV, as expected for a lobster-eye optical system. The deviations from the prediction of an ideal lobster-eye telescope are mostly caused by imperfections inherent in the manufacturing process of the MPO plates and the mounting, and the obscuration of the MPO supporting structures of the mirror assembly.

## 4. The LEIA Experiment

The LEIA instrument was successfully launched on 2022 July 27 carried by a solid-fueled "LiJian" rocket from Jiuquan satellite launch center in China, piggybacked onboard the SATech-01 satellite. With a total of 16 scientific instruments onboard, SATech-01 was developed by the Innovation Academy for Microsatellites of CAS. Figure 7 shows a picture of SATech-01 before launch, in which LEIA is sitting on top of
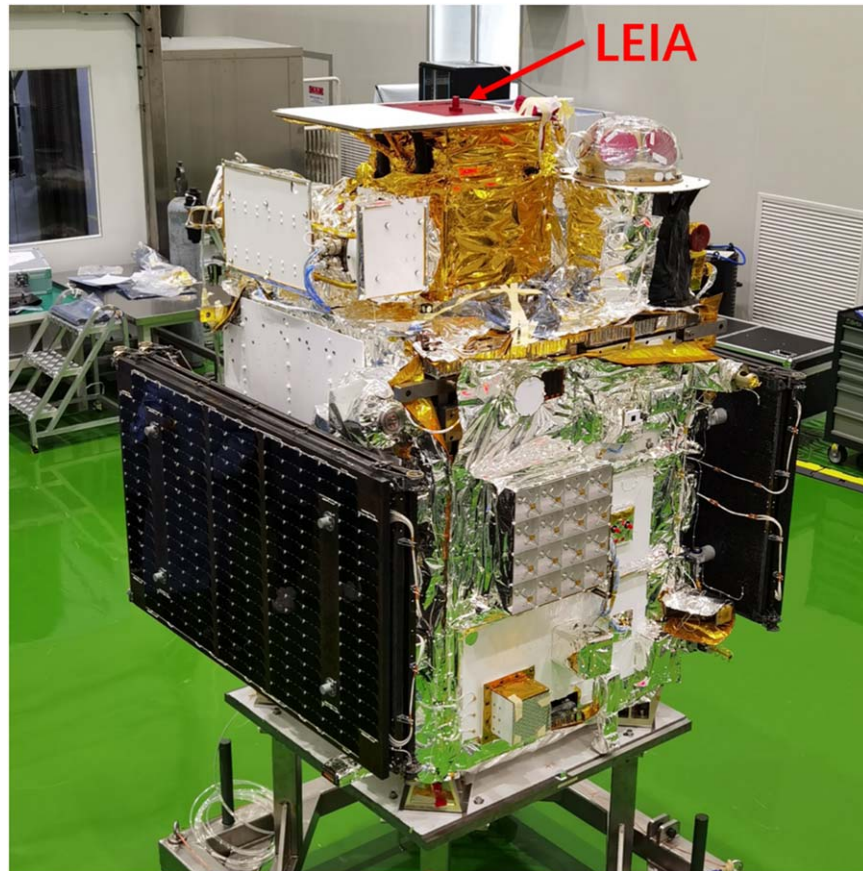
**Figure 7.** The photograph of the SATech-01 satellite.

the satellite. In addition to LEIA, there are two other instruments for astronomical research, the Solar Upper Transition Region Imager (SUTRI) (Bai et al. 2023) for solar observations in optical and High Energy Burst Searcher (HEBS) to detect gamma-ray bursts (S. L. Xiong et al. 2023, in preparation). The parameters of SATech-01 are listed in Table 2. The satellite has a total weight of 620 kg, a total power of 480 W and a storage capacity of 2 T bit. The satellite is in a Sun-synchronous orbit of 500 km height, with a 95 minute orbital period. The descending node of the orbit is 10:30 AM. The pointing accuracy is $0°\!.1$ and the stability is $1''\!.8$ per second during observation. The design life of the satellite is 2 yr.

LEIA was degassed in the first few days after launch. In the first two months of the satellite's test stage, all of the 16 scientific instruments were powered on in turn. LEIA had a test period of 4 days at this stage. After about two months of commissioning and experiments with the satellite platform and the payloads, the majority of the instruments completed their tasks and became inactive, while the three astronomical instruments continued to operate for further testing as well as long-term scientific observations.

To protect the instrument and minimize the impact of radiation from the Sun, a Sun-avoidance angle of $90°$ is set for LEIA. LEIA observations are carried out during the orbital phase in the Earth's shadow, while on the day side the SUTRI instrument (whose FoV is always perpendicular to that of LEIA) is operating and pointed to the Sun. Figure 8 features a schematic sketch of the satellite and LEIA operation in one orbit. To prevent the Sun from entering the LEIA FoV during satellite slew, the satellite starts slewing 10 minutes after entering the Earth's shadow region and 10 minutes before leaving it. The maximum slew time of the spacecraft is 10 minutes. Only pointed observation mode has been adopted so far, and usually only one patch of the sky is observed in one orbit.

The instrument stops collecting data in regions where extraordinarily high detector background is produced by charged particles in orbit, mainly the South Atlantic Anomaly (SAA) region and near the south and north polar regions of the Earth. Moreover, in-orbit data show that, within considerable intervals of one orbit the particle background dominates the detected events of the detector, and have to be discarded. Only data taken in the low geomagnetic latitude regions are not
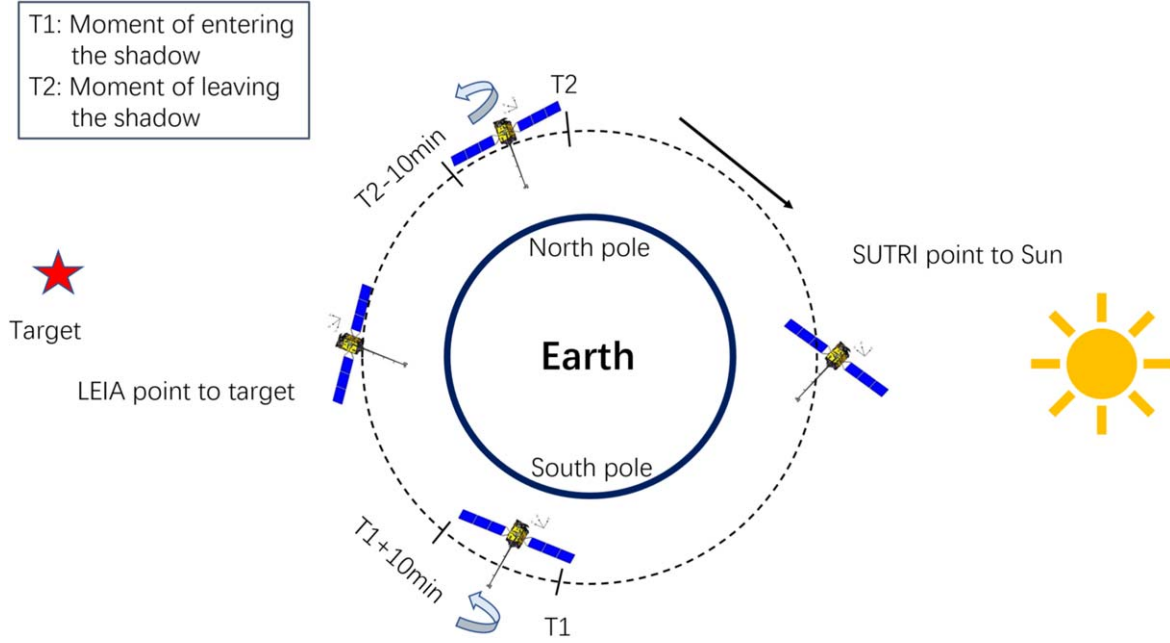
**Figure 8.** The operation mode of the SATech-01 satellite.

**Table 2**
Basic Specifications of the SATech-01 Satellite

| Orbit | 500 km |
|---|---|
| Descending node | 10:30 A.M. |
| Total weight | 620 kg |
| Power | 480 W |
| Pointing accuracy | $0°1$ |
| Star tracker accuracy | $3''(3\sigma)$ |
| Stability | $1''8\ s^{-1}$ |
| Storage capacity | 2 T bits |
| Number of instruments | 16 |
| Dimensions | $\phi$ 963 mm ($Y$) $\times$ 966 mm ($Z$) $\times$ 1306 mm ($X$) |
| Lifetime | 2 yr |
| Launch date | 2022 July 27 |

subject to high particle background. When all of those factors are taken into account, the useful observation time usually ranges from 10 to about 15 minutes per orbit. The data on backgrounds induced by charged particles in LEIA observations are being analyzed and will be presented elsewhere. There are about 10 orbits per day available for LEIA observations.

There are usually four telemetry orbits per day for the command uplinking and two orbits for mass data downloading,

each with a link time of about 10 minutes. The observation schedule commands are uploaded during these four orbits. In normal operation, the observation schedule is formulated once per week, and the corresponding command is uploaded every day. An urgent observation requirement could be approved in less than 2 hr and could be uploaded in the next control orbit as soon as possible. The general data rate for LEIA is about 5 GB per day. Figure 9 depicts the data flow chart of the LEIA instrument. The raw data will be sent to the ground station by the $X$-band antenna during the command orbit. The trigger message could be sent to the ground data center immediately, and the maximum delay is less than 2 minutes.

LEIA produces two types of scientific data. The event data record the X-ray events detected and are used for scientific research. The raw images of the detector can also be recorded and downloaded to periodically examine the status of the CMOS sensors and the performance of the optical blocking layers. These two types of data could not be recorded simultaneously.

## 5. Initial Results, In-orbit Calibration and Current Status

### 5.1. Initial Results

In the first two months of operation in orbit, the instrumental PV and calibration were performed. In this section, we present selected initial results in more detail obtained in the PV phase, in addition to the first-light images released in Zhang et al. (2022). As the first lobster-eye wide-field focusing X-ray
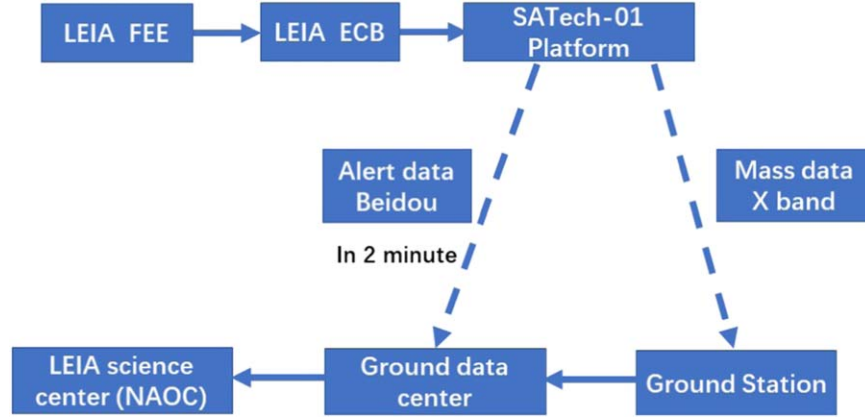
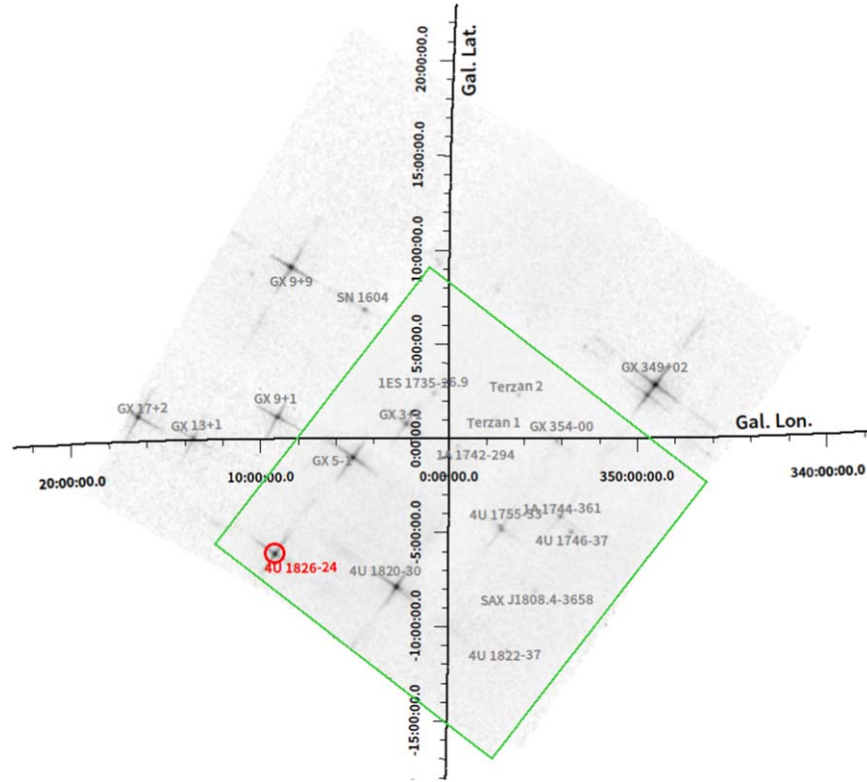**Figure 9.** The data flow chart of the LEIA instrument.



**Figure 10.** A stacked image of seven LEIA observations of the Galactic Center with a total exposure time of 4652 s. All of the detected sources are known X-ray sources in this image. The green box shows the FoV of LEIA.

telescope, LEIA's performance was tested by taking images of a number of celestial objects. The targets observed in the early PV phase include the Galactic Center where the number density of bright X-ray sources is the highest, Sco X-1, Cas A, the Cygnus Loop and the Crab Nebula. The images of the first-light observations, including part of the Galactic Center region, Sco X-1 and the Cygnus Loop nebula, have been presented in

Zhang et al. (2022). To further demonstrate the unique wide-field imaging capability of lobster-eye MPO optics, we show in Figure 10 the X-ray image of part of the Galactic Center region, covering $28° \times 28°$. The image is mosaicked and stacked from data taken in seven LEIA observations with a total exposure time of 4652 s, with part of the FoVs overlapping each other. In just several observations of about 10 minutes each, the Galactic
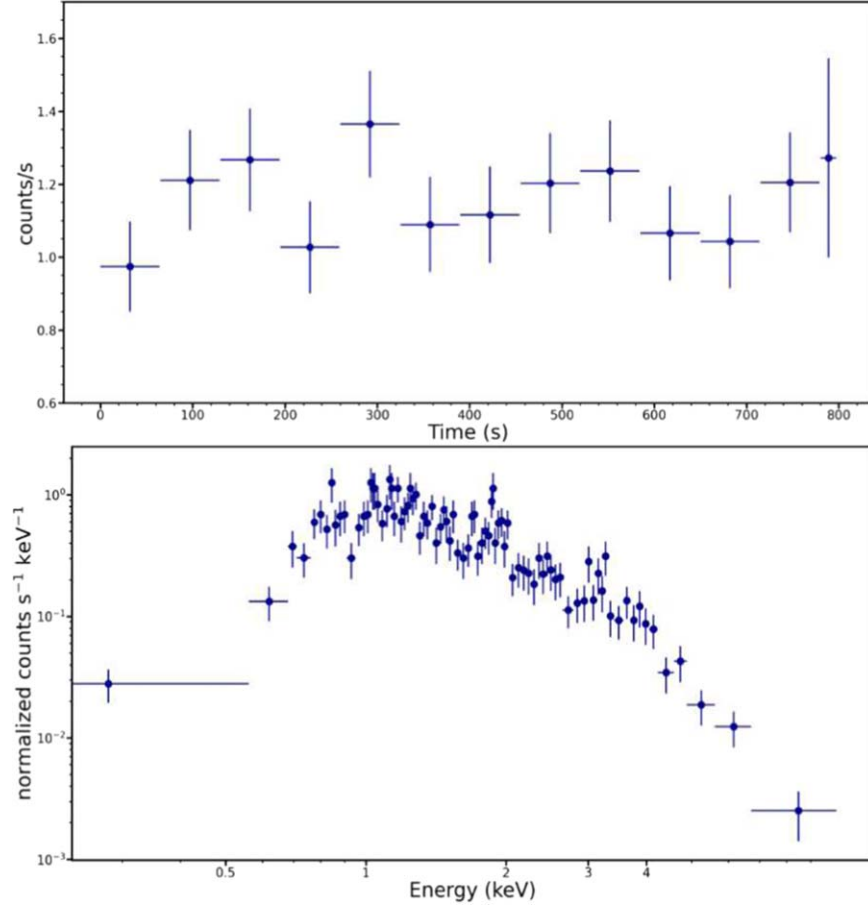
**Figure 11.** The light curve and the spectrum of X-ray binary 4U 1826-24 obtained in one pointing observation (marked by a red circle in Figure 10).

bulge region spanning $28° \times 28°$ can be covered, with about 11 X-ray sources detected. The image shows no significant variations in the imaging quality or the effective area across the FoV, as predicted based on the results of the on-ground calibration. However, quantitative comparisons with the on-ground calibration have to await results of extensive in-orbit calibration, for which the observations have been performed and are still to be completed.

Furthermore, the fast readout and spectroscopic capability of the CMOS sensors make it possible to obtain the short-timescale X-ray light curves and energy spectra of bright sources during one pointed observation. One such example is shown in Figure 11, where the X-ray light curve and spectrum of the X-ray binary 4U 1826-24 can be obtained simultaneously in one of the observations in Figure 10. These results demonstrate the great potential of monitoring X-ray sources and transients in the Galactic bulge region by a lobster-eye telescope such as LEIA with frequent visits.

The imaging quality of LEIA has been examined with observations of Sco X-1 in the directions at the centers of one quadrant, giving PSF of $3'.6$ (FWHM). This has excellent

consistency with the PSF values measured in on-ground calibration. It is interesting that the X-ray image of diffuse X-ray sources can also be produced by lobster-eye optics. Example images of Sco X-1 and Cygnus Loop are presented in Figure 4 in Zhang et al. (2022).

The onboard triggering system and the algorithm were also tested during the PV phase. Their performance is still under evaluation and the result will be presented elsewhere in the future (Y. Liu et al. 2023, in preparation).

An observation of 3C 382 was conducted. The observed image is displayed in Figure 12. There are 15 net X-ray photons with a significance of $6.3\sigma$ in a diameter of an $8'$ region in a 604 s observation. The flux of 3C 382 is about 3.4 to $4.2 \times 10^{-11} \, \mathrm{erg \, s^{-1} \, cm^{-2}}$ in 2–10 keV (Ursini et al. 2018). In spite of the uncertainty introduced by the unknown X-ray spectral parameters of the quasar at the time of the observation, the result indicates that LEIA has a sensitivity consistent with that estimated from the simulations. A systematic analysis of the LEIA sensitivity is on-going with more observations targeting faint X-ray sources and will be presented elsewhere.
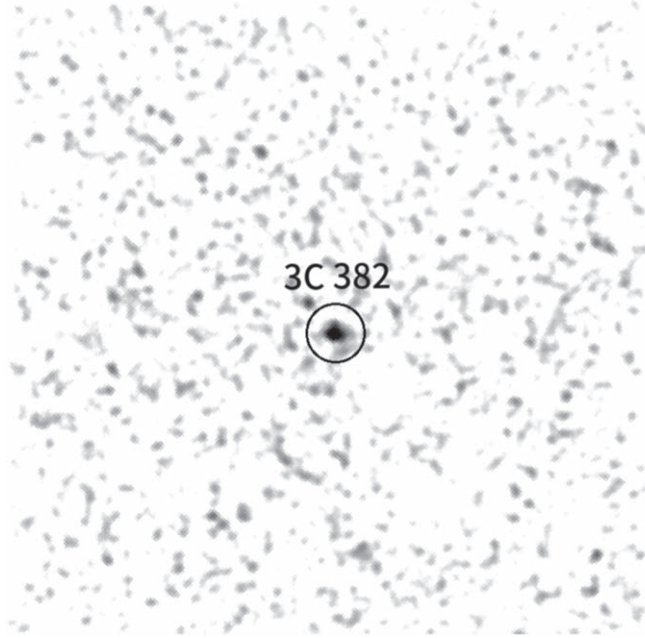
**Figure 12.** The observed image of the quasar 3C 382, with 15 net source counts detected in the 604 s observation.

## 5.2. In-orbit Calibration

The in-orbit calibration campaign was mainly carried out from 2022 October 1 to 2022 December 17 and some of the calibration observations are still on-going. For the calibration of the effective areas and the source positioning offsets, the Crab Nebula is the calibration source. The Crab Nebula has been observed a large number of times, and each time the telescope pointing is adjusted in such a way that the Crab image falls onto a given position (direction) on a $22 \times 22$ grid within the entire FoV. In this way the effective areas and positioning offsets can be calibrated for a large number of directions of the FoV. For other directions not sampled, interpolation should be performed. For the calibration of the energy resolution and gain of the detectors, Cas A is the primary source, and the calibration is still on-going. The data of the in-orbit calibration observations of LEIA are still under extensive analysis and the results will be presented in a separate paper.

## 5.3. Current Status

Since the start of its operation in 2022 August, LEIA has been operating in orbit for about 6 months so far. Preliminary analysis shows that there was no significant degradation in its performance over the 6 months of operation.

From 2022 October, LEIA has started test scientific observations, in addition to the on-going calibration observations of the Crab Nebula and other tests. There are several observation programs being undertaken, including monitoring the Galactic plane, the Large and Small Magellanic Clouds (LMC, SMC), and surveys of selected high Galactic latitude sky regions. However, the scientific productivity of LEIA could be severely limited by a number of factors. The first is the relatively short observable time intervals (10–15 minutes) largely owing to high particle background in the unfavorable orbit of SATech-01. Besides, several of the daily orbits will be unavailable for observations due to data telemetry of the satellite and other constraints. Second, the latency of receiving data from data taking is about one day at the moment, which is too long for some short-lived transients to be identified and their alerts to be triggered. The lack of an onboard telescope also hampers quick follow-ups once a fast transient is detected.

Albeit with these drawbacks, LEIA has been conducting scientific observations since 2022 October and has been accumulating an increasing amount of data. As of the time of writing, LEIA has made a total of 1542 pointed observations, covering a total sky region of 36,000 square degrees. The average exposure time of one pointed observation is 868 s and the total observing time amounts to 1.34 Ms. An extensive analysis of this data set is to be carried out, especially when the in-orbit calibration is completed and the calibration data are fully analyzed. Here we only highlight several preliminary results. Thanks to the large FoV, LEIA has surveyed the Galactic plane 10 times, covering a region of $l = 0–270$ and $l = 345°–360°$ and $b = -15°–15°$. The FoV of LEIA can fully cover LMC in one snapshot, and it also carried out monitoring observations of LMC 90 times in the past several months. On 2023 January 20, an outburst of LMC X-4 with an increase of its X-ray flux by a factor of 30 was detected by LEIA (Li et al. 2023). LEIA is also performing a large-scale sky survey at high
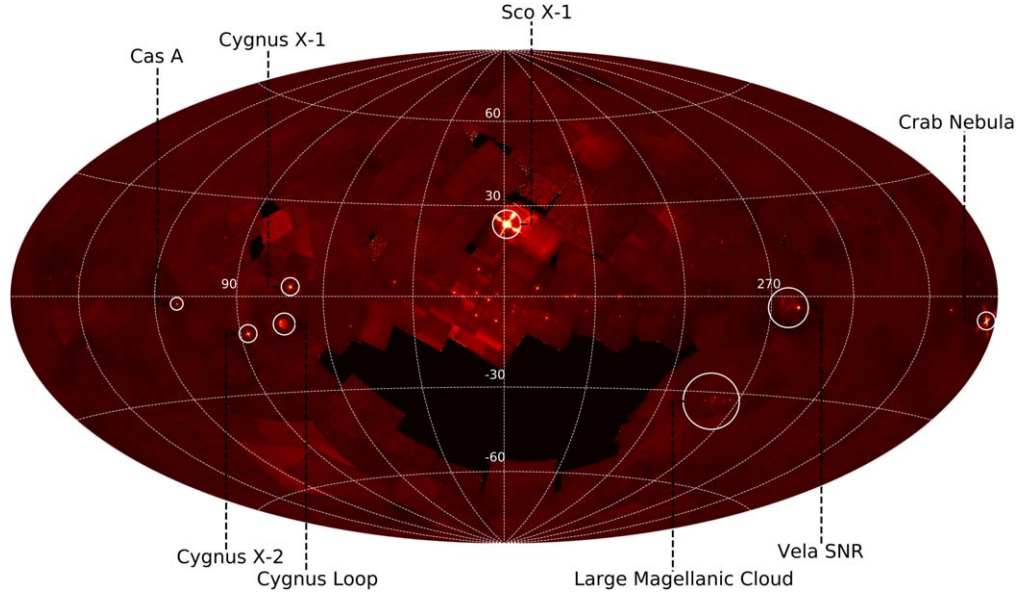
**Figure 13.** The sky coverage of LEIA observations as of 2023 April (in Galactic coordinates).

Galactic latitude regions, aiming at detecting bright extragalactic variables and transients. So far, more than half of the entire sky has been covered, mostly with one pointing lasting for 10–15 minutes. Figure 13 illustrates the sky coverage by LEIA in Galactic coordinates until 2023 April. It is expected that with the motion of the Sun in the sky, the rest of the sky regions will be covered in the next several months.

LEIA has also detected a number of transient events or candidates. As an example, during one of the calibration observations of Crab, a bright transient source LXT 221107A, the very first one for LEIA, was detected in the same FoV (Ling et al. 2022). Follow-up observations with Swift/XRT also detected the source and enabled precise localization and identification with a nearby star HD 251108 at a distance of $497 \pm 6$ pc (Gaia Collaboration et al. 2022). The peak luminosity observed with LEIA was $1.5^{+0.4}_{-0.2} \times 10^{34}$ erg s$^{-1}$, making it one of the brightest stellar X-ray flares. A detailed analysis of this flaring event is underway. In addition, several other fast X-ray transients or candidates were also detected (Cheng et al. 2022). More transients and variables are expected to be detected in future observations.

When the onboard triggering system is turned on, it will search for transients automatically. Once a transient is found, the alert message of the source will be transmitted to the ground by the Beidou navigation system in real time. The information about the new transient will be examined at the Einstein Probe Science Center based at NAOC. For genuine transient sources of potentially high scientific interest, alerts will be publicly released to the wider astronomical community to call for multiwavelength follow-up observations.

## 6. Conclusions

As a pathfinder for the WXT of the EP mission of the CAS, LEIA is a lobster-eye X-ray imager, which was launched on 2022 July 27 onboard CAS's SATech-01 satellite. The primary goals of LEIA are to verify the in-orbit performance of the state-of-the-art MPO and X-ray CMOS devices, the two novel technologies that are key to the EP mission. With an FoV of 346 square degrees, it is the first wide-FoV X-ray focusing telescope operating in orbit. Previous on-ground calibrations demonstrated that the imaging PSF (4′–8′) and effective areas (2–3 cm$^2$ for the central spot at 1.25 keV) are largely uniform with only mild variations across the entire FoV except at the edges. Thus it is a truly wide-FoV X-ray focusing telescope with only little vignetting effects. LEIA has a nominal soft X-ray bandpass of 0.5–4 keV.

Since its operation in orbit, extensive testing and calibration observations have been performed in the following months. So far, the instrument works mostly normally as far as its main functions are concerned, focusing on imaging, spectroscopy and timing. Preliminary results derived from observations taken in this period suggest that both the MPO and CMOS sensors adopted have been working well. The measured FoV, PSF and effective areas are very consistent with those measured in previous on-ground calibrations. The typical detecting sensitivity of LEIA is $2$–$3 \times 10^{-11}$ erg s$^{-1}$ cm$^{-2}$ for a 1000 s exposure, depending on the background level. This value is roughly consistent with the simulated result based on on-ground calibration data. In-orbit calibrations have been carried out and the data analysis will be completed in the near future. Preliminary results show that no significant degradation of the

performance has been observed in the past 5 months of observation.

These results demonstrate that the lobster-eye MPO, CMOS sensors and the entire telescope have been proved to work, and the goals of LEIA have largely been achieved. This is also the first time, to our knowledge, that CMOS sensors have been applied to X-ray astronomical detection in space. The LEIA experiment will pave the way for the development of present and future X-ray missions using lobster-eye and CMOS technologies.

The available observing intervals are relatively short, typically about 10–15 minutes for each usable orbit, while the latency of data telemetry is somewhat long. In spite of this, the wide FoV combined with the moderate angular resolution and sensitivity enabled by lobster-eye MPO make LEIA a promising soft X-ray wide-field monitor. This has been evidenced by the detection of several transients and outbursts by LEIA in the past several months of operation. LEIA is expected to carry out monitoring observations of the Galactic plane, LMC/SMC and selected sky regions at high Galactic latitudes in the following 1.5 yr or so which is within its expected lifetime.

## Acknowledgments

## References

Angel, J. R. P. 1979, ApJ, 233, 364

Brunton, A. N., Martin, A. P., Fraser, G. W., & Feller, W. B. 1999, NIMPA, 431, 356

Bai, Xianyong, Tian, Hui, Deng, Yuanyong, et al. 2023, RAA, 23, 065014

Chapman, H. N., Nugent, K. A., & Wilkins, S. W. 1991, RScI, 62, 1542

Chen, Y., Cui, W., Han, D., et al. 2020, Proc. SPIE, 11444, 114445B

Cheng, H. Q., Ling, Z. X., Liu, Y., et al. 2022, ATel, 15834, 1

Collier, M. R., Porter, F. S., Sibeck, D. G., et al. 2015, RScI, 86, 071301

Fraser, G. W., Brunton, A. N., Lees, J. E., Pearson, J. F., & Feller, W. B. 1993, NIMPA, 324, 404

Fraser, G. W., Lees, J. E., Pearson, J. F., Sims, M. R., & Roxburgh, K. 1992, Proc. SPIE, 1546, 41

Freyberg, M. J., Bräuninger, H., Burkert, W., et al. 2005, ExA, 20, 405

Gaia Collaboration, Vallenari, A., Brown, A. G. A., et al. 2022, arXiv:2208.00211

Hudec, R., Sveda, L., Pína, L., et al. 2017, Proc. SPIE, 10567, 1056719

Kaaret, P., Geissbuehler, P., Chen, A., & Glavinas, E. 1992, ApOpt, 31, 7339

Li, D. Y., Sun, H., Pan, H. W., et al. 2023, ATel, 15871, 1

Ling, Z. X., Liu, Y., Zhang, C., et al. 2022, ATel, 15748, 1

Peele, A. G., Nugent, K. A., Rode, A. V., et al. 1996, ApOpt, 35, 4420

Ursini, F., Petrucci, P. O., Matt, G., et al. 2018, MNRAS, 478, 2663

Wang, L., Qin, L., Cheng, J., et al. 2020, ITAS, 30, 1

Wang, Y., Zhao, Z., Hou, D., et al. 2022, arXiv:2210.15840

Wilkins, S. W., Stevenson, A. W., Nugent, K. A., Chapman, H., & Steenstrup, S. 1989, RScI, 60, 1026

Willingale, R., Pearson, J. F., Martindale, A., et al. 2016, Proc. SPIE, 9905, 99051Y

Wu, Q., Jia, Z., Wang, W., et al. 2022, PASP, 134, 035006

Yuan, W., Amati, L., Cannizzo, J. K., et al. 2016, SSRv, 202, 235

Yuan, W., Zhang, C., Chen, Y., & Ling, Z. 2022, in The Einstein Probe Mission, ed. C. Bambi & A. Santangelo, Handbook of X-ray and Gamma-ray Astrophysics, ed. C. Bambi & A. Santangelo (Berlin: Springer), 1

Yuan, W., Zhang, C., Ling, Z., et al. 2018, Proc. SPIE, 10699, 1069925

Zhang, C., Ling, Z. X., Sun, X. J., et al. 2022, ApJL, 941, L2

Zhao, D., Zhang, C., Ling, Z., et al. 2018, Proc. SPIE, 10699, 106995N

Zhao, D., Zhang, C., Yuan, W., et al. 2017, ExA, 43, 267